Journal of University of Science and Technology Beijing
Volume 9, Number 5, October 2002, Page 372

Materials

Crack initiation ahead of piled-up of dislocations emitted from a mode II blunt crack

Caifu Qian[1], *Wuyang Chu*[2], *and Lijie Qiao*[2]

1) Department of Mechanical Engineering, Beijing University of Chemical Technology, Beijing 100029, China
2) Department of Materials Physics, University of Science and Technology Beijing, Beijing 100083, China
(Received 2002-01-24)

Abstract: In situ tensile tests in a transmission electron microscope (TEM) show that dislocations emitted from a mode II crack tip will form a inverse piled-up group after equilibrium or a double piled-up group when they meet a obstruction, *e.g.*, grain boundary or second phase. A microcrack can initiates in front of the piled-up group of dislocations. Micromechanics analysis shows that dislocations emitted from a mode II blunt crack tip can form a inverse piled-up or double piled-up group, depending upon the applied stress intensity factor K_{IIa}, lattice friction stress τ_f and the distance of the obstruction from the crack tip L. The maximum normal stress in front of the double piled-up group which is located at the direction of $\alpha = -64°$ increases with the increase in the stress intensity K_{IIa} and the obstruction site L, and the decrease in the friction stress τ_f. When it increases to equate the cohesive strength, a microcrack will initiate in front of the piled-up group.

Key words: mode II blunt crack; dislocation emission; crack initiation; double piled-up group

[*This project was financially supported by the special funds for the Major State Basic Research Projects (G19990650), Visiting Scholar Foundation of Key Laboratory of the Ministry of Education PRC and by the NNSF of China.*]

1 Introduction

In situ tensile tests in transmission electron microscope (TEM) showed that for metallic materials, whether ductile (such as pure iron, brass and stainless steels) or brittle (such as Fe_3Al, TiAl, Ti_3Al+Nb), a inverse piled-up group of dislocations and a dislocation-free zone (DFZ) formed after dislocation emission reaching to an equilibrium, and with further increasing the load microcracks nucleated in the DFZ and/or at the blunted crack tip [1-4]. It is possible only when hundreds of atomic bonds break simultaneously. To achieve this, local concentrated stresses must be equal to or greater than the cohesive strength of materials [5]. Therefore, stress distribution ahead a blunt crack tip after dislocation emission must be analysed [6,7]. Qian *et al* [8] calculated the stress distribution ahead of an elliptic crack tip after dislocation emission and reaching to an equilibrium configuration under mode I loading, and found that the first peak stress at the blunt crack tip decreases while the second peak stress in DFZ increases with increasing K_{Ia}. Microcrack will initiate when the peak stress is equal to the cohesive strength.

When the applied stress intensity is large, the dislocation emitted from a crack tip will meet an obstruction, like grain boundary and second phase, before equilibrium, and be piled-up against the obstruction. After equilibrium, the front dislocations emitted from a crack tip will be piled-up against the obstruction and the latter dislocations inversely ahead of the crack tip, and hence a double piled-up configuration forms. Dewald *et al.* indicated that the size of the DFZ depend upon the position and intensity of the obstruction [9]. However, they did not investigate the stress distribution of the double piled-up configuration and the initiation of microcrack.

For a smooth specimen, the stresses ahead of a piled-up group have been calculated and if the length of the piled-up group is long enough, the maximum normal stress could equate to the cohesive strength, resulting in initiation of microcrack in front of the piled-up group [10]. For a double piled-up configuration in which the front dislocations are piled-up against the obstruction and the latter dislocations are inversely piled up ahead of the crack tip, the stress distribution is not available. In this case, it isn't known whether a microcrack can initiate in front of the piled-up group. In this article the existence of the double piled-up group of dislocations and microcrack initiating in front of the piled-up group will be firstly recognized through in situ tensile tests in

Corresponding author: Wuyang Chu **E-mail**:wychu@mater.ustb.edu.cn

TEM. Microcrack initiating in front of a double piled-up group was experimentally observed in front of a mode II blunt crack, thus a mechanical analysis was performed for a mode II blunt crack after emitting dislocation and forming a double piled-up configuration.

2 In situ tensile tests in TEM

The material used in the tensile test was ASTM Grade 2 Ti of 99.2% purity. The annealed strip of 0.2 mm thickness was thinned to 30-50 μm mechanically. The foil specimens for TEM were prepared by jet electropolishing with an electrolyte of 50 mL $HClO_3$+350 mL CH_3OH+150 mL butanol. The in situ tensile test was carried out in H-800 TEM. Cracks can be generated from the edge of the hole generated during electropolishing.

Many dislocations would be emitted from a preexisting crack tip during loading. If the load is small and keeps a constant, the emitted dislocations will reach an equilibrium before meeting a obstruction, as shown in **figure 1**. In figure 1, the edge dislocations BC are emitted along the crack plane, and inversely piled-up ahead of the crack tip A. This is a mode II crack. No dislocations were observed in the region of AB when extensively tilting the specimen, therefore, AB is a dislocation free zone (DFZ). When the applied load is high, more dislocations are emitted and it is possible that the front dislocations will meet an obstruction and be piled-up against the obstruction, as shown in **figure 2** and **3**. In figure 2, the front dislocations emitted from a mode II crack tip are piled up against a second phase F, the latter dislocations are inversely piled up ahead of the crack tip A, and a microcrack MN initiations ahead of the double piled-up group. In figure 3, the front dislocations C are piled up against a grain boundary GG, the latter dislocations inversely piled up ahead of the crack tip A, and microcracks a, b, and c initiate in the DFZ of AB.

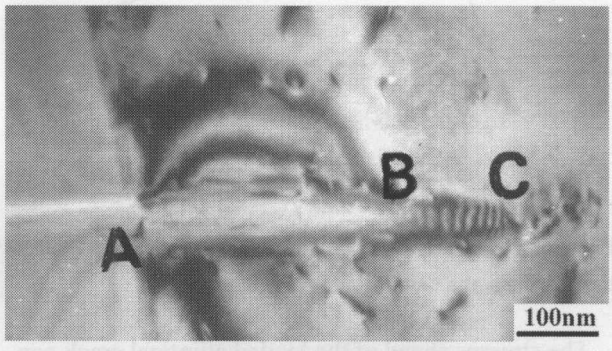

Figure 1 Invesely piled-up group ahead of a mode II crack. A —crack tip; BC—dislocations; AB—dislocation-free zone.

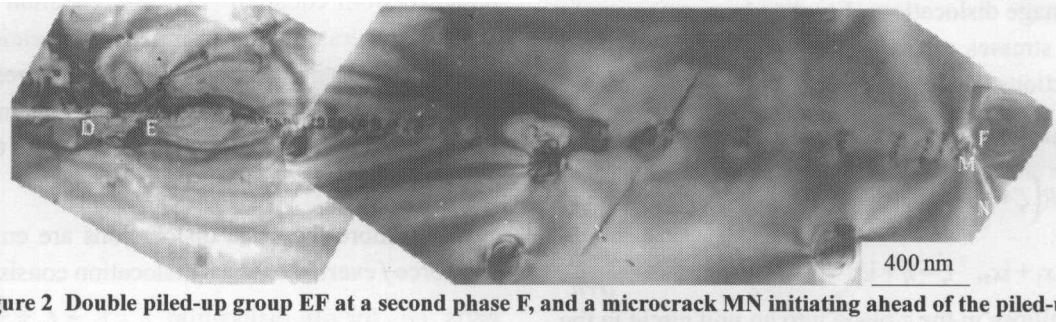

Figure 2 Double piled-up group EF at a second phase F, and a microcrack MN initiating ahead of the piled-up.

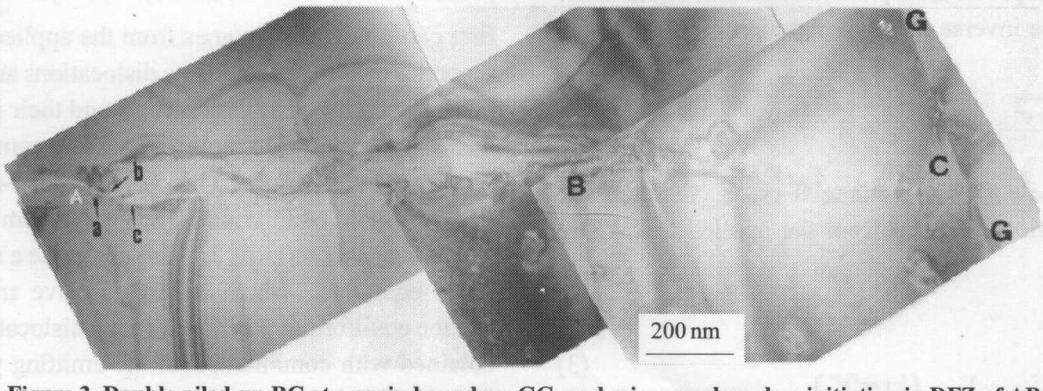

Figure 3 Double piled-up BC at a grain boundary GG, and microcracks a, b, c initiating in DFZ of AB.

3 Stress distribution ahead of a double piled-up group of dislocations emitted from a mode II blunt crack

3.1 Calculation procedure

Measuring in TEM under an enlargement factor of one million showed that the crack tip generated during electropolishing has curvature radius of 3-8 nm after loading. When the semi-major axis and semi-minor axis of an elliptic are chosen as $a = 5\times10^6\boldsymbol{b}$ and $h = 10^4\boldsymbol{b}$ ($\boldsymbol{b}$ is the Burgers vector), respectively, the elliptic crack with the radius of $\rho = h^2/a \approx 5$ nm can simulate a real

crack observed in TEM. Assume that the obstruction, at which dislocations emitted from the blunt crack tip are piled-up, is a tilt sub-boundary with a misorientation of 23° and edge dislocation period of 2.5***b***, as shown in **figure 4**. The applied stress is τ_a, so that this is a mode II crack in order to simulate the cracks shown in figure 1 and 2. When the applied stress intensity $K_{IIa}=\tau_a\sqrt{\pi a}$ exceeds the critical stress intensity for dislocation emission, edge dislocations will be emitted along the crack plane, and piled-up against the tilt sab-boundary if increasing further the K_{IIa}.

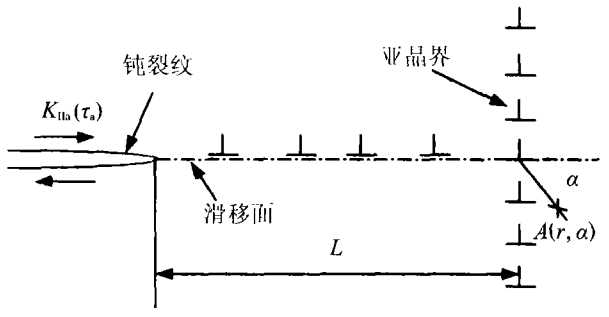

Figure 4 Schematic plot of mode II blunt crack and dislocation piled-up at a sub-boundary.

The stresses ahead of the loaded elliptical crack consist of three parts. The first part comes from the applied load, the second from all dislocations, and the third from all image dislocations. For the plane strain condition, the stresses can be calculated by two complex stress functions [8,12], *e.g.*, equation (3) in reference 8.

The conformal mapping function [11] is:

$$z=\omega(\zeta)=R\left(\zeta+\frac{m}{\zeta}\right) \tag{1}$$

where $z=x_1+ix_2$, $\zeta=\eta+i\xi$, $R=\frac{a+h}{2}$ and $m=\frac{a-h}{a+h}$, maps the ellipse in the z plane into an unit circle in the ζ plane. The inverse mapping function of equation (1) is:

$$\zeta=\frac{z+\sqrt{z^2-c^2}}{2R} \tag{2}$$

where $c^2=a^2-h^2$. For a mode II crack, the complex stress functions resulted from the applied load τ_a are [12]:

$$\begin{cases}\phi(\zeta)=\dfrac{\tau_a R}{\zeta}\\ \psi(\zeta)=i\tau_a R\left[\zeta-\dfrac{1}{m\zeta}+\dfrac{(1+m^2)\zeta}{m(\zeta^2-m)}\right]\end{cases} \tag{3}$$

The surfaces of the elliptic crack are stress-free, which requires the complex stress functions of an edge dislocation and its image dislocation satisfy the following boundary condition on the unit circle in ζ plane [8],

$$\phi_d(\sigma)+\phi_i(\sigma)+\frac{\sigma^2+m}{\sigma(1-m\sigma^2)}\overline{[\phi_d(\sigma)+\phi_i(\sigma)]}+\overline{\psi_d(\sigma)}+\overline{\psi_i(\sigma)}=0 \tag{4}$$

where ϕ_d and ψ_d are the complex stress functions of the edge dislocation which are available[12], and ϕ_i and ψ_i that of its image dislocation. In equation (4), $|\sigma|=1$. Consequently, the complex stress functions for the image dislocations are obtained as:

$$\phi_i(\zeta)=-\gamma\ln\left(\zeta-\frac{1}{\bar{\zeta}_d}\right)+\gamma\ln\zeta-\gamma\ln(\zeta-m/\zeta_d)+\frac{\bar{\gamma}}{\zeta_d\bar{\zeta}_d(\bar{\zeta}_d^2-m)}\cdot$$
$$[\zeta_d(1+m\bar{\zeta}_d^2)-\bar{\zeta}_d(\zeta_d^2+m)]\cdot\frac{1}{\zeta-1/\bar{\zeta}_d} \tag{5}$$

$$\psi_i(\zeta)=-\bar{\gamma}\ln(\zeta-\frac{1}{\zeta_d})+\bar{\gamma}\ln\zeta-\bar{\gamma}\ln(\zeta-m/\zeta_d)+\frac{\gamma}{\zeta_d\bar{\zeta}_d(\zeta_d^2-m)}\cdot$$
$$[\bar{\zeta}_d(\zeta_d^2+m^3)-m\zeta_d(\bar{\zeta}_d^2+m)]\frac{1}{\zeta-m/\zeta_d}+$$
$$\gamma\frac{\zeta(1+m\zeta^2)}{(\zeta^2-m)(\zeta-1/\bar{\zeta}_d)}-\zeta\frac{1+m\zeta^2}{\zeta^2-m}\phi_0'(\zeta) \tag{6}$$

where $\phi_0(\zeta)=\phi_i(\zeta)+\gamma\ln\left[\zeta-\frac{1}{\bar{\zeta}_d}\right]$, $\gamma=\frac{\mu(b_2-ib_1)}{4\pi(1-\mu)}$, z_d is the position of the edge dislocation with Burgers vector $\boldsymbol{b}=b_1+ib_2$. If transforming $\phi_i(\zeta)$ and $\psi_i(\zeta)$ from ζ plane back to z plane, have:

$$\begin{cases}\phi_i'(z)=\phi_i'(\zeta)/\omega'(\zeta)\\ \psi_i'(z)=\psi_i'(\zeta)/\omega'(\zeta)\end{cases} \tag{7}$$

After the complex stress functions $\phi_i(z)$ and $\psi_i(z)$ are obtained from equation (7) and equation (2), the stresses generated from the image dislocation can be calculated. The numerical solution of the stresses ahead of the loaded elliptic crack after emitting many dislocations can be obtained through summing the three parts of stresses.

When more than one dislocations are emitted, the slip force f exerted on each dislocation consists of three parts, *i.e.*, for i-th dislocation, $f_i=f_{ia}+f_{ii}+\sum_{m\neq i}^{n}f_{im}$. The first part on the right comes from the applied load, the second is due to its own image dislocations and the third is induced by other dislocations and their image dislocations. Dislocation motion must overcome the friction force $\boldsymbol{b}\tau_f$. Therefor, when $|f_i|\leq\boldsymbol{b}\tau_f$, the i-th dislocation will be in equilibrium. The equilibrium equations for all dislocations (i=1, 2, ···, n) comprise a set of nonlinear equations, which is hard to solve analytically. But the equilibrium position for each dislocation can be obtained with combination of the emitting process as follows. Suppose there already exist n dislocations around the blunt crack tip, now put a new dislocation (n+1-th) at the point (initiating point) of 2***b*** from the crack tip in the slip plane. If the slip force on the new dislocation is larger than the friction force, the dislocation will move forward from the crack tip, meaning a dislocation is emitted. At this time, the n old disloca-

tions may be no longer in equilibrium. Thus, the slip force on each dislocation has to be calculated again and when the slip force on a dislocation is larger than the friction force, the dislocation will move forward or backward from the crack tip along the slip plane until the slip force is less than the friction force and the dislocation is at an equilibrium position again. When all $n+1$ dislocations are at equilibrium, a new round of dislocation emission begins. If the slip force on a new dislocation at the initiating point is less than the friction force, the emission process stops and the calculation terminates. Therefore, for a given K_{IIa}, the number and positions of emitted dislocations are obtained, so are the DFZ size w and the stress fields of dislocations in front of the blunt crack tip.

3.2 Calculation results

Calculation indicates that the distribution of emitted dislocations depends upon τ_a/τ_f and the distance of the sub-boundary (obstruction) from the crack tip L. If τ_a/τ_f is small and L is large, the dislocations emitted from the crack tip are a few and can not reach as far as the sub-boundary. In this case, the dislocations are inversely piled-up ahead of the crack tip and not piled-up against the sub-boundary. If both τ_a/τ_f and L are small, the dislocations emitted are a few, but can reach the sub-boundary and be plied-up. If both τ_a/τ_f and L are large, many dislocations are emitted and the front dislocations will be piled-up at the sub-boundary, and the latter dislocations inversely piled-up ahead of the crack tip. In **figure 5**, there are two typical calculation results. Figure 5 shows that when $\tau_a=\tau_f=0.006\mu$, $K_{IIa}=1.063\mu\boldsymbol{b}^{1/2}$, $L=10^4\boldsymbol{b}$, 45 dislocations are emitted and inversely piled-up ahead of the crack tip but do not piled-up at the sub-boundary. Figure 1 corresponds to this case. Figure 5 shows also that when $\tau_a=0.008\mu$, $K_{IIa}=1.418\mu\boldsymbol{b}^{1/2}$, $\tau_a/\tau_f=4$ and $L=10^4\boldsymbol{b}$, 110 dislocations are emitted and piled-up at the sub-boundary, *i.e.*, a double piled-up group forms. Figure 2 and 3 correspond to this case. Therefore, the larger the drive force of dislocation emission τ_a or K_{IIa} is, the smaller the lattice friction stress τ_f and the distance of the obstruction from the crack tip L are, the easier to form the double piled-up group of dislocations is.

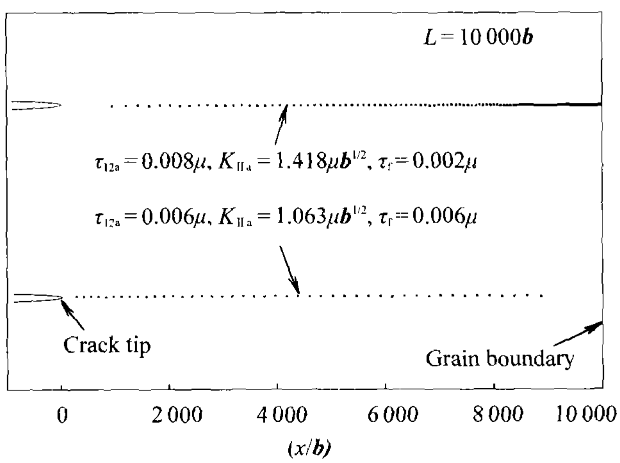

Figure 5 Two kind of distributions of dislocation emitted from the blunt crack ahead of the sub-boundary.

To calculate the stress distribution ahead of the double piled-up group, the point of intersection between the sub-boundary and the extension of the crack is chosen as the origin of the coordinate axes. The stress field of the sub-boundary only extends to a distance equal to edge dislocation period of 2.5$\boldsymbol{b}$ [10], and hence can be ignored when calculating the stresses at the distance r≥3$\boldsymbol{b}$. Therefore, the normal stress σ_n at point A ($r\geq 3\boldsymbol{b}$, α) shown in figure 4 only results from the crack and the piled-up group of dislocations. The normal stress at the position of $r=3\boldsymbol{b}$, $\sigma_n(r=3\boldsymbol{b}, \alpha)$, *vs* the angle α is shown in **figure 6**. Figure 6 shows that the maximum normal stress σ_{max} locates at the direction of $\alpha=-64°$ and $\sigma_{max}=0.113\mu$ when $\tau_f=0.002\mu$, $K_{IIa}=1.418\mu\boldsymbol{b}^{1/2}$ and $L=10^4\boldsymbol{b}$, which equates to or exceeds the cohesive strength. The maximum normal stress at $\alpha=-64°$, $\sigma_n(r, \alpha=-64°)$ decreases with increasing the distance from the obstruction, as shown in **figure 7**. With incre-

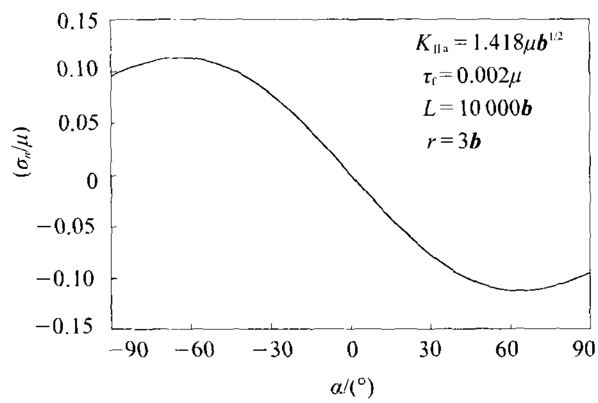

Figure 6 The normal stress ahead of a piled-up group at the position of r=3b *vs* the orientation of α.

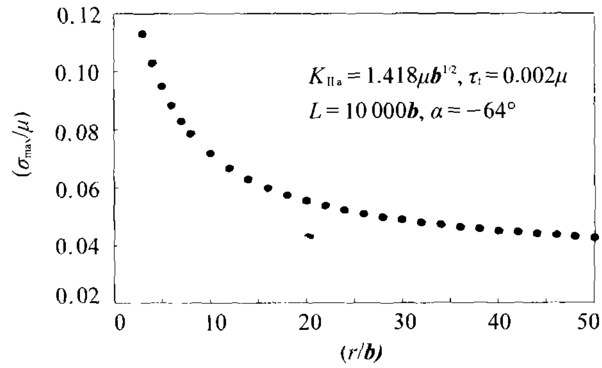

Figure 7 The maximum normal stress at the orientation of $\alpha=-64°$ *vs* the distance from the obstruction r.

asing K_{IIa}, the stress induced by the crack increases, and the number of dislocations emitted as well as the stress induced by the piled-up group increase, too. As a result, the maximum normal stress ahead of the piled-up group increases with the increases in K_{IIa}. For example, when $\tau_f=0.006\mu$, $L=10^4\boldsymbol{b}$, $r=3\boldsymbol{b}$,

$$\sigma_{\max}=-0.525+1.80K_{\mathrm{IIa}}-2.013K_{\mathrm{IIa}}^2+0.749K_{\mathrm{IIa}}^3 \quad (8)$$

where the units of $\sigma_{\max}$ and K_{IIa} are μ and $\mu\boldsymbol{b}^{1/2}$, respectively. The number of dislocations emit, and then $\sigma_{\max}$ decrease with increasing τ_f. For example, when $K_{\mathrm{IIa}}=0.709\mu\boldsymbol{b}^{1/2}$, $L=10^4\boldsymbol{b}$, $r=3\boldsymbol{b}$,

$$\sigma_{\max}=0.028\,8-6.223\tau_f+589.6\tau_f^2-1\,837\tau_f^3 \quad (9)$$

where the unit of τ_f is μ. With increasing the length of the plied-up group L, the stress field induced by the crack, σ_c, decreases because the point A (r, α) is farther away from the crack tip, but that induced by the piled-up group σ_D, increases because of more dislocations emitted. If L is shorter, *e.g.*, $L<6\times10^3\boldsymbol{b}$, the effect of σ_c on $\sigma_{\max}$ will be larger than that of σ_D, and then $\sigma_{\max}$ decreases with the increase in L. For example, when $K_{\mathrm{IIa}}=0.709\mu\boldsymbol{b}^{1/2}$, $\tau_f=0.002\mu$, $L<6\times10^3\boldsymbol{b}$, $r=3\boldsymbol{b}$,

$$\sigma_{\max}=9.318\times10^{-3}-7.79\times10^{-7}L+6.5\times10^{-11}L^2 \quad (L<6\times10^3) \quad (10)$$

where the unit of L is $\boldsymbol{b}$. If L is longer, *e.g*, $L>10^4\boldsymbol{b}$, the effect of σ_D on $\sigma_{\max}$ will be larger than that of σ_c, and hence $\sigma_{\max}$ increases with the increase in L, as shown in **figure 8**. In figure 8, $K_{\mathrm{IIa}}=0.709\mu\boldsymbol{b}^{1/2}$, $\tau_f=0.002\mu$, $r=3\boldsymbol{b}$ and the variation of $\sigma_{\max}$ with L is as follows:

$$\sigma_{\max}=6.636\times10^{-3}+9.9\times10^{-9}L+9\times10^{-12}L^2 \quad (L>10^4\boldsymbol{b}) \quad (11)$$

For a real polycrystal, the size of sub-grain and grain is larger than $10^4\boldsymbol{b}$, and the average distance between large second phases as the obstruction is in general larger than $10^4\boldsymbol{b}$, too. Therefore, $\sigma_{\max}$ will increase with the increase in the length of the piled-up group L. Figure 8 shows also that the number of emitted dislocations n increases with increasing L.

The emitted dislocations shield the crack from external load by introducing shielding stress intensity factors K_{IIs}. So the effective stress intensity factor K_{IIf} presiding at the crack tip is $K_{\mathrm{IIf}}=K_{\mathrm{IIa}}+K_{\mathrm{IIs}}$. With dislocation emission, the shielding effect of the emitted dislocations increases and the effective stress intensity factor K_{IIf} decreases, as shown in **figure 9**. Figure 9 indicates also that both K_{IIf} and the size of dislocation-free zone (DFZ) decrease with the number of emitted dislocations.

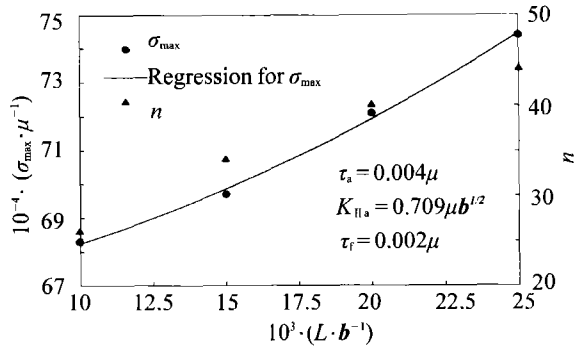

Figure 8 The maximum normal stress $\sigma_{\max}$($r=3\boldsymbol{b}$, $\alpha=-64°$) and the number of emitted dislocations *vs* the distance of the obstruction from the crack tip L.

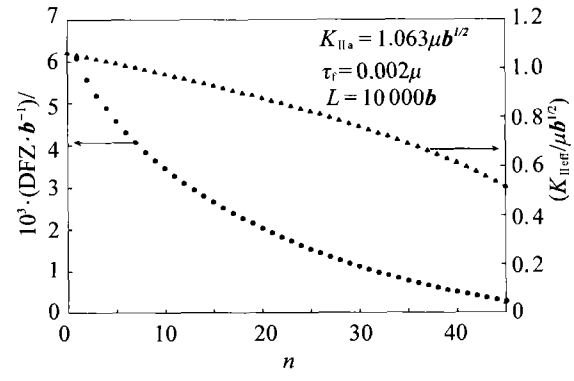

Figure 9 The effective stress intensity K_{IIf} and the size of dislocation-free zone DFZ *vs* the number of emitted dislocations n.

4 Discussion

Figure 9 indicates that the size of DFZ decreases with the increase in the number of the equilibrium dislocations emitted, which is consistent with the experiment result observed in TEM. For example, DFZ=250 nm when the equilibrium dislocations n=15, as shown in figure 1, and DFZ=80 nm when $n\approx80$, as shown in figure 2.

Calculation shows that the maximum normal stress $\sigma_{\max}$ depends upon the applied stress intensity K_{IIa} (see equation (8)), the friction stress τ_f (see equation (9)) and the length of the piled-up group L (see equation (10)). When K_{IIa} or/and L is large enough, the maximum normal stresses in a certain region ahead of the piled-up, *e.g.*, $r\leq10\boldsymbol{b}$, are equal to or larger then the cohesive strength $\sigma_{\mathrm{th}}=(0.08\text{-}0.1)\mu$ [13]. In this case, all atom bounds in this region of $r\leq10\boldsymbol{b}$ will be broken, and then a microcrack with the size of $10\boldsymbol{b}$ will initiate. It can propagate immediately because of the existence of the large normal stress $\sigma_{\max}$. Figure 2 indicates that there is a microcrack MN ahead of the piled-up group along the direction of $\alpha=-64°$, in which the normal stress has a maximum value (see figure 6). During extending in

TEM, the preexisting blunt crack is mode I or mode I+II. When a complex crack of mode I+II is along one of the slip planes, the edge dislocation can only be emitted along the crack plane, as shown in figure 1 and 2. In this case, the calculation results corresponding to a mode II crack can be used. If the complex crack is not along the slip plane and the component of mode I is larger, the normal stress in DFZ can be calculated based on the mode I crack, *e.g.*, [8]

$$\sigma_{max}=(-0.116+16\tau_f-4350\tau_f^2)+(0.128+13.4\tau_f)K_{Ia}-0.029K_{Ia}^2 \quad (12)$$

where the uite of τ_f and σ_{max} is μ and that of K_{Ia} is $\mu b^{1/2}$. Therefore, with the increase in K_{Ia}, the normal stress in the DFZ can equate to the cohesive strength, resulting in initiation of microcrack in the DFZ, as shown in figure 3. In a word, the experimental results observed in TEM can be qualitatively explained based on the mechanical analysis.

5 Conclusions

(1) Experiment and analysis show that the dislocations emitted from a blunt mode II crack tip can form a double piled-up group after meeting a obstruction.

(2) The maximum normal stress in front of the double piled-up group, which is located at the direction of $\alpha=-64°$, increases with increasing the stress intensity K_{IIa} and the length of the piled-up group L, and with decreasing the friction stress τ_f.

(3) A microcrack initiates along the direction of the maximum normal stress when it raise to equate the cohesive strength, and it has been proved through in situ tensile test in TEM.

Acknowledgment

Discussions with Dr. Tong-Yi Zhang of the Hong Kong University of Science & Technology are greatly acknowledged.

References

[1] Q.Z. Chen, W.Y. Chu, and C.M. Hsiao, In suit TEM observation of nucleation and bluntmess of nanocracks in thin crystals of 310 stainless steel [J], *Acta Metall. Mater.*, 43(1995), p.4371.

[2] L.J. Qiao, X. Mao, and Q.Z. Chen, Nanometer-scale crack initiation and propagation behavior of Fe_3Al-based intermetallic alloy [J], *Metall. Mater. Trans.*, A26(1995), p.1461.

[3] Y. Zhang, Y.B. Wang, and W.Y. Chu, The in-situ TEM observation of microcrack nucleation in titanium aluminide [J], *Scripta Metall Mater.*, 30(1994), p.541.

[4] Q. Z. Chen, K.W. Gao, Y. Zhang, and W.Y. Chu, Nucleation, blunting or propagation of a nanocrack in dislocation-free zone of thin crystals [J], *Fatigue Frac Eng. Mater Struc.*,21 (1998), p.981

[5] S.M. Ohr, An electron microscope study of crack tip deformation and its impact on dislocation theory of fracture [J], *Mater. Sci. Eng.*, 59(1983), p.1.

[6] H. Huang and W.W. Gerberich, Crack-tip dislocation emission arrangements for equilibrium [J], *Acta Metall.*, 40 (1992), p.2883.

[7] T. Zhu, W. Yang, and T. Gao, Quasi-cleavage processes dirven by dislocation piloups [J], *Acta Mater.*, 44(1996), p. 3049.

[8] C.F. Qian, L.J. Qiao, and W.Y. Chu, Stress distribution and effective stress intensity factor of a blunt crack after dislocation emission [J], *Sci. in China* (in Chinese), E43(2000), p. 421.

[9] D.K. Dewald, T.C. Lee, I.M. Rdoertson, and H.K. Birnhaum, Dislocation structures ahead of advancing cracks [J], *Scripta Metall*, 23(1989), p.1307.

[10] J. Friedel, *Dislocation* [D], Pergamon press, New york, 1964, p.260.

[11] N.I. Muskhelishvili, *Some Basic Problens of Mathematical Ttheory of Elasticity* [D], Noordhoff Ltd, Groningen, The Netherlands, 1963.

[12] T.Y. Zhang, and J.C.M. Li, Image forces and shield effects of an edge dislocation near a finite length crack [J], *Acta Metall Mater.*, 39(1991), p.2739.

[13] G. P. Cherepanov, *Mechanics of Brittle Fracture* [D], McGraw-Hill Inter Book Comp, New York, 1977, p.27.